Food Chemistry: X 21 (2024) 101058

Contents lists available at ScienceDirect

Food Chemistry: X

journal homepage: www.sciencedirect.com/journal/food-chemistry-x

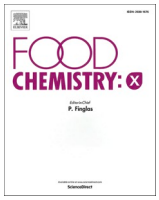

Structural and digestive characters of a heteropolysaccharide fraction from tea (*Camellia sinensis* L.) flower

Dan Chen [a], Ao Wang [a], Jialiang Lv [a], Chao Tang [a], Chang-hai Jin [a], Jun Liu [a], Xiaoxiong Zeng [b], Li Wang [c,*]

[a] College of Food Science and Engineering, Yangzhou University, Yangzhou 225127, Jiangsu, China
[b] College of Food Science and Technology, Nanjing Agricultural University, Nanjing 210095, Jiangsu, China
[c] Key Laboratory of Agricultural Product Fine Processing and Resource Utilization, Ministry of Agriculture and Rural Affairs, Anhui Engineering Laboratory for Agro-products Processing, College of Tea & Food Science and Technology, Anhui Agricultural University, Hefei 230036, Anhui, China

ARTICLE INFO

Keywords:
Tea flower
Polysaccharide
Structure
Digestibility
Bacteroides

ABSTRACT

Tea (*Camellia sinensis* L.) flower polysaccharides (TFPS) have various health-promoting functions. In the present work, the structure of a purified TFPS fraction, namely TFPS-1-3p, and its *in vitro* digestive properties were investigated. The results demonstrated that TFPS-1-3p was a typical heteropolysaccharide consisting of rhamnose (Rha), arabinose (Ara), galactose (Gal) and galacturonic acid (GalA) with a molecular weight of 47.77 kDa. The backbone of TFPS-1-3p contained → 4)-α-D-Gal*p*A(-6-OMe)-(1 → 4)-α-Gal*p*A-(1 → and → 4)-α-D-Gal*p*A(-6-OMe)-(1 → 2,4)-α-L-Rha*p*-(1 → linkages. The branch linkages in TFPS-1-3p contained → 6)-β-D-Gal*p*-(1→, →3,6)-β-D-Gal*p*-(1→, →5)-α-L-Ara*f*-(1 → and → 3,5)-α-L-Ara*f*-(1 →. Subsequently, TFPS-1-3p could not be degraded under simulated human gastrointestinal conditions but could be of use to human fecal microbes, thereby lowering the pH and increasing the production of short-chain fatty acids (SCFAs) of the gut microenvironment and altering the composition of the gut microbiota. The relative abundance of *Fusobacterium_mortiferum Megasphaera_elsdenii_DSM_20460, Bacteroides thetaiotaomicron*, *Bacteroides plebeius* and *Collinsella aerofaciens* increased significantly, potentially contributing to the degradation of TFPS-1-3p.

1. Introduction

Dietary polysaccharides are distributed in a wide range of plants, animals, and microorganisms. It is widely recognized that dietary polysaccharides with low toxicity have multiple benefits for health, such as antioxidant, anti-obesity, anti-diabetic, antitumor, hepatoprotective, immunomodulatory and probiotics-like activities, and thus have received extensive attention (Chen, et al., 2021; Chen, et al., 2022; Lee, Kim, & Park, 2022). Physico-chemical and function characteristics of dietary polysaccharides vary with their sources, extraction methods and structural characteristics (Chen, et al., 2022). Polysaccharides can be structurally classified into homogeneous and heterogeneous polysaccharides in view of their monosaccharide compositions (Yao, Wang, Yin, Nie, & Xie, 2021). Homopolysaccharides are composed of a uniform type of sugar monomer, such as starch, cellulose, or glycogen. Heteropolysaccharides are comprised of two or more different monosaccharide units linked by linear or branched glycosidic linkages. However, the restricted use of polysaccharides as dietary supplements has been limited to date because of their low purity, high heterogeneity, and ambiguous structure–function relationships (Tang, et al., 2019). Understanding the chemical structure of dietary polysaccharides remains challenging, which severely limits their application (Chen, et al., 2022; Yao, et al., 2021).

Most dietary polysaccharides have complex glycosidic linkages and are difficult for the body's digestive enzymes to break down. The human lower gastrointestinal tract is colonized by a complex community of trillions (10^{14}) of individual microorganisms. This complex ecosystem is largely driven by a broad structural diversity of indigestible dietary polysaccharides (Briggs, Grondin, & Brumer, 2021). For example, carbohydrate-active enzymes (CAZymes) that target the carbohydrate-rich human diet and indigestible dietary polysaccharides present in the gut are encoded by many members of the gut flora. Gut microbes grow on complex and diverse polysaccharides, and gut microbial taxa may compete or cooperate in glycosyl catabolism, thus forming a complex ecological network across different trophic niches (Tang, et al., 2019). This quantitative and functional diversity of polysaccharide

* Corresponding author.
E-mail address: Lwang@ahau.edu.cn (L. Wang).

https://doi.org/10.1016/j.fochx.2023.101058
Received 11 September 2023; Received in revised form 25 November 2023; Accepted 6 December 2023
Available online 10 December 2023

utilization systems determines a taxon's polysaccharide utilization profile, be it a "specialist" or "generalist" (Briggs, et al., 2021). Gut microbiota ferment non-digestible polysaccharides to produce short-chain fatty acids (SCFAs) and other metabolites that are captured by the colonic endothelium and released into the circulation, where they can have multiple beneficial effects on hosts (Frampton, Murphy, Frost, & Chambers, 2020). Maintaining a balanced gut ecology has been implicated in the regulation of human diseases (de Vos, Tilg, Van Hul, & Cani, 2022; Fan & Pedersen, 2021; Hasain, et al., 2020), and is one of the important operational roles of numerous dietary polysaccharides, accompanied by their own metabolic processes in the body.

In the past two decades, tea (*Camellia sinensis* L.) flowers have been found to be a valuable new resource that has attracted much attention in Japan and China (Chen, et al., 2020). In this context, tea flower polysaccharides (TFPS) are typical substances with various health-promoting functions, including antioxidant, anti-obesity, hepatoprotective, anti-allergic, and immunomodulatory activities (Chen, et al., 2019). Our previous work revealed that a purified polysaccharide fraction, named TFPS-1-3p, could enhance the immunoreactions in cyclophosphamide-induced immunosuppression mice and could serve as a potential immunomodulator to improve host's health (Chen, et al., 2019). Given that TFPS-1-3p consisted of carbohydrates (33.96 ± 0.04 %, glucose equivalent), uronic acids (78.79 ± 1.51 %, glucuronic acid equivalent), and proteins (0.75 ± 0.14 %), and was made up of the following galacturonic acid (GalA), arabinose (Ara), galactose (Gal), and rhamnose (Rha) with a molar ratio of 74.05: 14.56: 7.92: 3.47 (Chen, et al., 2019). However, the structure of TFPS-1-3p remains elusive. Therefore, the structure of TFPS-1-3p was characterized using high-performance gel permeation chromatography (HPGPC), methylation analysis, and nuclear magnetic resonance (NMR) spectroscopy. Additionally, the digestive properties of TFPS-1-3p were investigated *in vitro* under simulated human gastrointestinal and colonic conditions. The aim of this work is to provide a basic structural characterization and digestive properties for further exploitation of TFPS-1-3p.

2. Materials and methods

2.1. Materials and chemicals

Dried tea flowers (variety, Longjing 43, harvested in November 2019 in Hangzhou, Zhejiang, China) were made available by the Department of Tea Science, Zhejiang University (Hangzhou, China). DEAE-Fast Flow and Sephadex G-100 were acquired by GE Healthcare Life Sciences. 3, 5-Dinitrosalicylic acid (DNS) was acquired by Sinopharm Chemical Reagent Co., Ltd. (Shanghai, China). Glucose was acquired by Aladdin Chemical Reagent Co., Ltd. (Shanghai, China). α-Amylase (from human saliva), gastric lipase, and pancreatin were acquired by Sigma Chemical Co., Ltd. (St. Louis, MO, USA). Pepsin, trypsin, and bile salt were bought by Solarbio Science & Technology Co., Ltd. (Beijing, China). All other reagents used were of at least analytical grade.

2.2. Preparation of TFPS-1-3p

The preparation of TFPS-1-3p was in accordance with our report (Chen, et al., 2019). Dried flowers were pulverized and pre-treated twice with 80 % aqueous ethanol at 1:20 (w/v). The pre-treated dried powder of tea flowers was then extracted twice with a distilled water (1:25, w/v) at 96 °C for 4 h each, and then centrifuged (3000 × *g*, 15 min) to collect the supernatants, and after concentration and precipitation with anhydrous ethanol, the crude TFPS extract was obtained. The crude TFPS was dissolved to filter through a 0.1 μm membrane (Merck Millipore, Germany), and the filtrate was precipitated with four times the volume of anhydrous ethanol to obtain the TFPS-1 extract after centrifugation (3000 × *g*, 15 min), dialysis, and lyophilization. Then, TFPS-1 (200 mg) was dissolved in deionized water (5.0 mL), applied to a DEAE-Fast Flow column (2.6 × 30 cm) and eluted stepwise with sodium chloride solution (0, 0.1, 0.3 and 0.5 mol/L) at a flow rate of 1.0 mL/min to obtain three fractions: TFPS-1–1, TFPS-1–2, and TFPS-1–3, respectively. TFPS-1–3 was further applied to a Sephadex G-100 column (1.6 × 100 cm) and eluted with 0.1 mol/L of NaCl solution at a flow rate of 15 mL/h, yielding TFPS-1-3p (Fig. S1).

2.3. The weight-average molecular weight (Mw) of TFPS-1-3p

The Mw of TFPS-1-3p was determined by HPGPC using an Agilent 1200 series instrument (Agilent Technologies, Santa Clara, CA, USA) fitted with a refractive index detector and a TSK-G4000PW$_{XL}$ column (7.8 mm × 300 mm, Tosoh Crop., Tokyo, Japan) (Yuan, et al., 2015). The mobile phase was 0.1 mol/L NaCl at a flow rate of 0.5 mL/min and the temperature of column oven was 35 °C. The Mw of TFPS-1-3p was estimated using standard dextran with known Mw of 6.2, 10, 21.7, 48.8, 113, 200, 348 and 736 kDa.

2.4. Methylation and GC–MS analysis

The glycosidic linkage of TFPS-1-3p was analyzed by methylation and the partially methylated alditol acetate (PMAA) derivatives were analyzed by GC–MS according to the reported method (Sims, Canachan, Bell, & Hinkley, 2018). TFPS-1-3p (5 mg) was dissoluted in deionized water (1 mL), combined with 1-cyclohexyl-3-(2-morpholinoethyl) carbodiimide metho-*p*-toluenesulfonate (1 mL, 100 mg/mL) and allowed to react for 2 h. After adding 1 mL of 2 mol/L imidazole, the solution was mixed with 1 mL of 30 mg/mL $NaBH_4$ or $NaBD_4$ and further reacted for 3 h and then terminated with acetic acid (100 μL). The resultant solution was dialyzed and lyophilized to provide carboxyl-reduced TFPS-1-3p for methylation. Carboxyl-reduced TFPS-1-3p was disbanded in 500 μL of dimethyl sulfoxide (DMSO), and mixed with 1 mg of NaOH and then allowed to react for 30 min. The solution was merged with 50 μL of methyl iodide and stored in the dark for 1 h, and then merged with 1 mL of water and 2 mL of dichloromethane. The phase of dichloromethane was collected, rinsed three times with water, and dried with nitrogen. The dried sample was merged with 100 μL of 2 mol/L trifluoroacetic acid solution and hydrolyzed at 121 °C for 90 min and then dried. This dried sample was mixed with 50 μL of 2 mol/L ammonium hydroxide and 50 μL of 1 mol/L $NaBD_4$ and allowed to react at room temperature for 2.5 h. Acetic acid (20 μL) was used to stop the reaction, and the solution was rinsed four times in methanol and dried under nitrogen. The dried sample was then mixed with acetic anhydride (250 μL) and reacted at 100 °C for 2.5 h. 1 mL of water and 500 μL of dichloromethane were added sequentially, and the phase of dichloromethane was harvested after three times washes with water and analyzed on a GC–MS (7890A-5977B, Agilent Technologies Inc., CA, USA) platform fitted with a BPX70 column (30 m × 0.25 mm × 0.25 μm, SGE, Australia). The separation ratio was 10:1. Carrier gas was supplied at a flow rate of 1.0 mL/min using high purity helium. The initial column oven temperature was 140 °C for 2.0 min, and the temperature was ramped to 230 °C with a 3 °C/min program and maintained for 3 min. Analyte was detected in the mass scan range (*m/z*) in full scan mode (SCAN): 30–600. According to the standardized data in the CCRC Spectral Database for PMAA derivatives, the glycosyl linkages of TFPS-1-3p were identified.

2.5. NMR analysis

TFPS-1-3p was suspended in 0.5 mL of deuterium oxide (D_2O, 99.9 % D) and freeze-dried three times to replace hydrogen. The 100 mg of dried sample was disoluted in 1 mL of D_2O, and 1D (^{1}H NMR and ^{13}C NMR) and 2D (homonuclear ^{1}H/^{1}H correlation spectroscopy (COSY), heteronuclear single-quantum coherence (HSQC), heteronuclear multiple-bond correlation (HMBC) and nuclear Overhauser effect spectroscopy (NOESY)) NMR spectra were acquired using a Bruker 600 MHz NMR instrument (Bruker Corp., Fallanden, Switzerland) at 298 K with 3-(trimethylsilyl) propionic-2,2,3,3-d4 acid sodium salt (TMSP) as the

internal standard. The NMR spectra were calibrated by HDO hydrogen δ_H at δ 4.70 ppm, methyl carbon of TMSP δ_C at δ −1.80 ppm, respectively.

2.6. In vitro digestive properties of TFPS-1-3p

The *in vitro* digestion properties of TFPS-1-3p were investigated under the simulated human gastrointestinal and colonic conditions.

2.6.1. Simulated oral and gastrointestinal digestion

The *in vitro* oral and gastrointestinal digestion was performed as protocol described with a few modifications (Brodkorb, et al., 2019). TFPS-1-3p was formulated 1:1 (wt/wt) with simulated salivary fluid (with or without salivary amylase) in the oral phase and incubated with stirring at pH 7 to simulate chewing of the meal. Simulated salivary fluid consisted of KCl (15.1 mmol/L), KH_2PO_4 (3.7 mmol/L), $NaHCO_3$ (13.6 mmol/L), NaCl, $MgCl_2(H_2O)_6$ (0.15 mmol/L), $(NH_4)_2CO_3$ (0.06 mmol/L), HCl (1.1 mmol/L), $CaCl_2(H_2O)_2$ (1.5 mmol/L), and salivary amylase (if present, 150 U/mL). The oral boluses were then formulated 1:1 (v/v) with simulated gastric fluid with or without gastric enzymes (pepsin and gastric lipase) and incubated for 6 at pH 3.0 h with stirring. Simulated gastric fluid consisted of KCl (6.9 mmol/L), KH_2PO_4 (0.9 mmol/L), $NaHCO_3$ (25 mmol/L), NaCl (47.2 mmol/L), $MgCl_2(H_2O)_6$ (0.12 mmol/L), $(NH_4)_2CO_3$ (0.5 mmol/L), HCl (15.6 mmol/L), $CaCl_2(H_2O)_2$ (0.15 mmol/L), pepsin (if present, 4000 U/mL) and gastric lipase (if present, 120 U/mL). Gastric chyle was then formulated 1:1 (v/v) with simulated intestinal fluid with or without pancreatin and bile salts, and incubated for another 6 h at pH 7. Simulated intestinal fluid consisted of KCl (6.8 mmol/L), KH_2PO_4 (0.8 mmol/L), $NaHCO_3$ (85 mmol/L), NaCl (38.4 mmol/L), $MgCl_2(H_2O)_6$ (0.33 mmol/L), HCl (8.4 mmol/L), $CaCl_2(H_2O)_2$ (0.6 mmol/L), pancreatin (if present, 200 U/mL) and bile salt solution (if present, 20 mmol/L). Each experiment was the subject of five independent replicates.

2.6.2. Simulated colonic fermentation

The *in vitro* colonic fermentation of TFPS-1-3p was investigated as the described protocol (Zhou, et al., 2018). The fresh feces were obtained from four healthy individuals (one female and three males) who were in good physical condition and off antibiotics for at least 3 months. Each fresh fecal samples were formulated equally and homogenized in autoclaved phosphate-buffered saline (0.1 mmol/L, pH 7.2) to obtain 10 % (w/v) fecal slurry. The supernatants were immediately transferred to anaerobic flasks as microbial donors after centrifugation (500 × *g*, 5 min). TFPS-1-3p was diluted 10:1 (w/v) with and the autoclaved nutrient medium and this mixture was diluted 9:1 (v/v) of microbial donors to start the fermentation phase in an anaerobic incubator (Yuejin Medical Optical Instruments Factory, Shanghai, China) and incubated at 37 °C for 24 h. The nutrient medium contained 2.0 g/L of yeast extract, 2.0 g/L of peptone, 0.1 g/L of NaCl, 0.04 g/L of K_2HPO_4, 0.01 g /L of $CaCl_2{\cdot}6H_2O$, 0.01 g/L of $MgSO_4{\cdot}7H_2O$, 2.0 g/L of $NaHCO_3$, 0.02 g/L of hemin, 0.5 g/L of cysteine HCl, 0.5 g/L of bile salts, 1.0 mg/L of resazurin, 0.2 % (v/v) of Tween 80 and 0.001 % (v/v) of vitamin K_1. Following the parallel conditions, equal amounts of fructooligosaccharide (FOS) and blank addition (BLK) were used as controls. The *in vitro* colonic fermentation phase at 0 h was maintained as the Origin group. Each experiment had five independent replications.

2.6.3. Changes of residual total carbohydrates and reducing sugar content during the simulated digestion and fermentation process

Total carbohydrate content was measured by the phenol–sulfuric acid method (Dubois, Gilles, Hamilton, Rebers, & Smith, 1956). Reducing sugar content was measured by DNS method (Miller, 1959). Glucose was used as the standard.

2.7. Effect of TFPS-1-3p on the gut microenvironment

The pH value during the colonic fermentation phase was detected using a pH meter (Mettler-Toledo Instruments Co., Ltd. Shanghai, China). The colonic fermentation chyme at 0 h and 24 h was centrifuged at 5000 × *g* for 5 min, the supernatants were obtained and formulated 1:1 (v/v) with 25 mmol/L 2-ethylbutyric acid (an internal standard). SCFAs was measured according to the reported method (Tian, et al., 2016). The mixture was formulated 1:1 (v/v) with 0.15 mmol/L of oxalic acid solution. 1 μL of the supernatant was obtained after centrifugation (5000 × *g*, 5 min) and injected onto an Agilent 6890 N GC system fitted with a HP-INNOWAX column (30 m × 0.25 mm × 0.25 μm, Agilent) and a flame ionization detector for the measurement of acetate, propionate, *n*/*i*-butyrate and *n*/*i*-valerate. Lactate was measured using a commercial assay kit (Nanjing Jiancheng Bioengineering Institute, China) according to the manufacturer's protocol. Meanwhile, colonic fermentation chyme precipitates at 0 h and 24 h were collected for microbial DNA extraction, followed by amplification of the V3-V4 regions of 16S rDNA on the Illumina MiSeq sequencing platform. Fecal microbiota composition was assessed based on QIIME microbiota analysis (Langille, et al., 2013).

2.8. Statistical analysis

All data are displayed as the mean ± standard deviation (SD) or box-whisker plots. Statistical significance between groups was analyzed by one-way ANOVA procedure followed by Tukey test using SPSS 22 software (IBM). A value of $p < 0.05$ was considered a significant difference. Linear discriminant analysis effect size (LEfSe) of microbial diversity was assessed on an online platform (https://huttenhower.sph.harvard.edu/galaxy/).

3. Results and discussion

3.1. Determination of the Mw of TFPS-1-3p

As shown in Fig. 1A, a single and symmetric peak was observed in the HPGPC chromatogram. Based on the calibration with dextran standard, the Mw of TFPS-1-3p was estimated to be 47.77 kDa. In another study, Han, et al. (2011) reported that the Mw of two polysaccharide fractions from tea flowers ranged from 10.71 to 167.5 kDa. The differences in Mw of TFPS could be associated with varieties, purification processes and test methods (Chen, et al., 2020).

3.2. Methylation analysis

Methylation analysis and GC–MS were used to investigate the glycosyl linkages of TFPS-1-3p. The glycosyl linkages of Rha, GalA, Gal, and Ara are displayed and summarized in Table 1 in accordance with the retention times and GC–MS mass fragments (Fig. S2 and S3, Supplementary Material). The peaks of PMAA derivatives of TFPS-1-3p were recognized as nine linkage modes including Ara*f*(1→, Gal*p*(1→, Gal*p*A (1→, →5)Ara*f*(1→, →2,4)Rha*p*(1→,→4)Gal*p*A(1→, →6)Gal*p*(1→, →3,5) Ara*f*(1→, and → 3,6)Gal*p*(1 → with the molar ratio of 3.17: 5.26: 7.10: 2.29: 3.27: 71.23: 2.32: 2.48: 2.88 (The calculated data are shown in Table S1, Supplementary Material). The proportions of Rha*p*, Gal*p*A, Gal*p* and Ara*f* in the methylation analysis were 1: 23.94: 3.20: 2.43. These results demonstrated that TFPS-1-3p was a typical heteropolysaccharide. The constituent sugar data indicated a higher proportion of Ara than the methylation data, which was likely due to issues with the methodological issues and resulting loss of some arabinosyl residues during the methylation procedure.

3.3. NMR spectra

To further explore the structure of TFPS-1-3p, 1D (^{1}H and ^{13}C) and

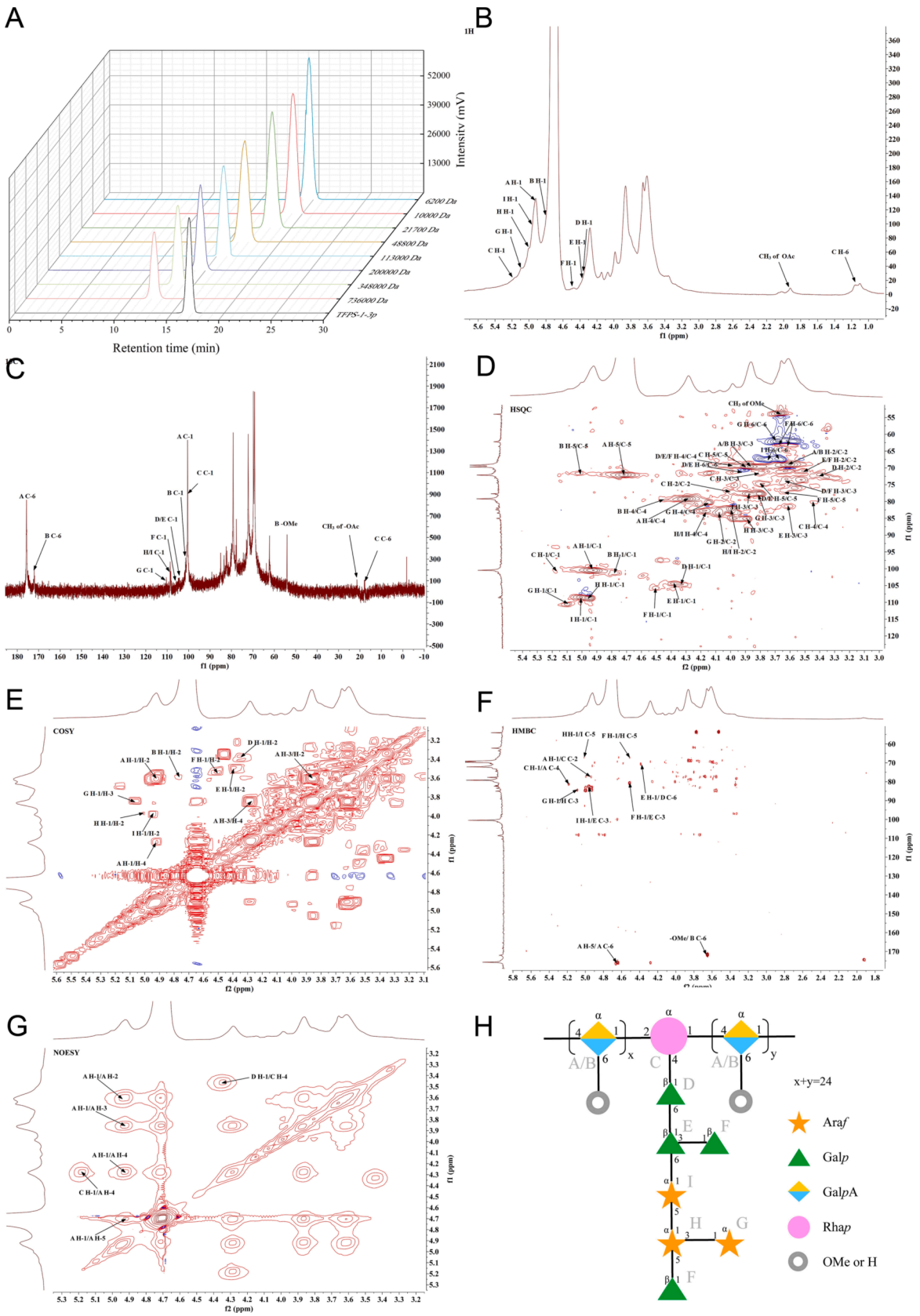

Fig. 1. Structural information identification of TFPS-1-3p. (A) HPGPC chromatogram, (B) ^{1}H NMR spectra, (C) ^{13}C NMR spectra, (D) HSQC NMR spectra, (E) COSY NMR spectra, (F) HMBC NMR spectra, (G) NOESY NMR spectra, and (H) hypothetical structure.

Table 1
Methylation analysis and mode of linkage of TFPS-1-3p.

Methylated alditol acetate	Type of linkage	Retention time	Molar ratio	Mass fragments (*m/z*)
1,4-di-*O*-acetyl-2,3,5-tri-*O*-methyl arabinitol	Ara*f*(1→	5.678	3.17	59, 71, 87, 102, 118, 129, 145, 161
1,5-di-*O*-acetyl-2,3,4,6-tetra-*O*-methyl galactitol	Gal*p*(1→	9.514	5.26	59, 71, 87, 118, 129, 145, 161, 205
1,5-di-*O*-acetyl-2,3,4,6-tetra-*O*-methyl galactitol	Gal*p*A (1→	9.514	7.10	59, 71, 88, 118, 131, 147, 163, 207
1,4,5-tri-*O*-acetyl-2,3-di-*O*-methyl arabinitol	→5)Ara*f* (1→	10.157	2.29	59, 87, 102, 118, 129, 162, 189
1,2,4,5-tetra-*O*-acetyl-6-deoxy-3-*O*-methyl rhamnitol	→2,4) Rha*p* (1→	11.951	3.27	74, 88, 102, 117, 130, 143, 160, 190, 203
1,4,5-tri-*O*-acetyl-2,3,6-tri-*O*-methyl galactitol	→4) Gal*p*A (1→	13.297	71.23	73, 87, 102, 118, 131, 175, 205, 235
1,5,6-tri-*O*-acetyl-2,3,4-tri-*O*-methyl galactitol	→6)Gal*p* (1→	14.976	2.32	59, 87, 102, 118, 129, 162, 189, 233
1,3,4,5-tetra-*O*-acetyl-2-*O*-methyl arabinitol	→3,5) Ara*f*(1→	18.207	2.48	85, 118, 127, 159, 201, 261
1,3,5,6-tetra-*O*-acetyl-2,4-di-*O*-methyl galactitol	→3,6) Gal*p*(1→	18.389	2.89	59, 74, 87, 101, 118, 129, 160, 189, 202, 234, 305

2D (COSY, HSQC, HMBC and NOESY) NMR spectra (Fig. 1B–F) were performed. As shown in Table 2, nine residues (labeled as A-I) were carefully distinguished. The ^{1}H NMR spectral signals in Fig. 1B were mainly between 3.0 and 5.5 ppm. Certain sugar residues or groups can be identified by the characteristic signals of ^{1}H NMR. For example, the methyl proton signal of 6-position deoxysugar is displayed in the high-field region of δ 0.8–1.4 ppm; the methyl proton signal of acetyl (CH_3COO– or -OAc) appears in the low-field region of δ 1.8–2.2 ppm; the methyl proton signal of methyl ester (–$COOCH_3$ or -COOMe) is located at δ 3.0–3.8 ppm (Yao, et al., 2021). The δ_H in the region of 4.4–4.95 ppm and 4.95–5.5 ppm was evidence for the presence of both α- and β-configured glycosidic linkages in TFPS-1-3p. In addition, the signals of the anomeric proton occurred primarily between 4.0 and 5.5 ppm, including δ4.92, 4.78, 5.17, 4.36, 4.4, 4.5, 5.09, 5.01, and 4.96 ppm equivalent to H-1 of A, B, C, D, E, I, F, and G. The ^{13}C NMR spectrum of the TFPS-1-3p was displayed in Fig. 1C, multiple anomeric carbons in the region of δ 90–111 ppm including δ100.64, 101.31, 104.36, 104.38, 105.89, 108.53, 108.68 and 110.61 corresponding to C-1 of C/A, B, D, E, F, H, I and G. It has been suggested that the reduced-terminal end groups belong to α-Gal*p*A and β-Gal*p*A based on the C-1 signal peaks at δ93.62 and 97.83 ppm, respectively (Petersen, Meier, Duus, & Clausen, 2008).

Detailed structural information could be obtained from the 2D NMR spectrum, a powerful technique for characterizing the structure of polysaccharides. Nine signals of the anomeric (carbon) atoms at 4.92 (100.64), 4.78 (101.31), 5.17 (100.64), 4.36 (104.36), 4.4 (104.38), 4.5 (105.89), 5.09 (110.61), 5.01 (108.53), and 4.96 (108.68) ppm from ^{1}H- and ^{13}C NMR spectra were found to be further resolved by 2D NMR spectroscopy. On the basis of the interpretation of the 1D, 2D NMR spectra and the data in the earlier works (Chen, et al., 2021; Yao, et al., 2021; Yuan, et al., 2020), nine types of glycosyl residues linkages in TFPS-1-3p have been assigned including → 4)-α-Gal*p*A-(1→, →4)-α-D-Gal*p*A-6-OMe-(1→, →2,4)-α-L-Rha*p*-(1→, →6)-β-D-Gal*p*-(1→, →3,6)-β-D-Gal*p*-(1→, terminal β-D-Gal*p*-(1→, terminal α-L-Ara*f*-(1→, →3,5)-α-L-Ara*f*-(1 → and → 5)-α-L-Ara*f*-(1 → and their signals were presented in Table 2.

The example of residue A, designated → 4)-α-Gal*p*A-(1→, was considered. In the HSQC spectrum (Fig. 1D), the signals of the anomeric protons and carbon atoms were observed at 4.92/100.64 ppm, indicating that residue A is in the α-configuration (Chen, et al., 2021; Yuan, et al., 2020). In the ^{1}H–^{1}H COSY spectrum (Fig. 1E), the cross peaks A H1/H2 (4.92/3.61), A H2/H3 (3.61/3.87) and A H3/H4 (3.87/4.27) were observed. Subsequently, the carbon signals including δ100.64, 69.11, 69.79, 79.46, and 72.12 ppm, which were assigned to C-1, C-2, C-3, C-4 and C-5 of residue A, could be further mapped in the HSQC spectrum (Fig. 1D). The cross peak δ 4.72/175.86 ppm of H-5 and C-6 was found in the HMBC spectrum (Fig. 1F). δ_C 175.86 ppm is the characteristic peak of the C-6 position in the non-esterified GalA residue. In this case, the chemical shifts of C-1 and C-4 moved to the lower panel, indicating that the residue was occupied at the C-1 and C-4 positions of the sugar nucleus according to certain published literature reports (Chen, et al., 2021; Chen, et al., 2022; Patova, et al., 2019; Petersen, et al., 2008; Yao, et al., 2021; Yuan, et al., 2020). Taken together, the sugar residue A has been recognized as → 4)-α-D-Gal*p*A-(1 →.

The δ_C 177 ppm was the characteristic peak of the C-6 position in the non-esterified GalA residue, and the characteristic peak of the C-6 position in the esterified GalA residue was located near δ_C 172.15 ppm (Petersen, et al., 2008). In the HSQC spectrum (Fig. 1D), the signal peak at δ 3.66/54.16 ppm was found. The signal at δ_H 3.66 ppm was the methyl proton of the methyl ester (-COOMe), and the characteristic peak

Table 2
^{1}H and ^{13}C chemical shifts from identified 2D NMR spectra of TFPS-1-3p.

Glycosyl residues	H1	H2	H3	H4	H5	H6a	H6b	OMe
	C1	C2	C3	C4	C5	C6		
A → 4)-α-Gal*p*A-(1→	4.92	3.61	3.87	4.27	4.72			
	100.64	69.11	69.79	79.46	72.12	175.86		
B → 4)-α-D-Gal*p*A-6-OMe-(1→	4.78	3.58	3.87	4.44	5.02			3.66
	101.31	69.26	69.29	79.8	71.65	172.15		54.17
C → 2,4)-α-L-Rha*p*-(1→	5.17	3.98	3.79	3.43	3.87	1.12		
	100.64	77.24	71.81	80.13	69.81	17.82		
D → 6)-β-D-Gal*p*-(1→	4.36	3.4	3.63	3.97	3.79	3.61	3.90	
	104.36	72.19	73.29	69.55	74.82	70.22		
E → 3,6)-β-D-Gal*p*-(1→	4.4	3.48	3.61	4.01	3.79	3.61	3.90	
	104.38	71.2	81.51	69.55	74.82	70.22		
F β-D-Gal*p*-(1→	4.5	3.52	3.63	3.97	3.63	3.61	3.66	
	105.89	71.09	73.65	69.55	76.63	63.26		
G α-L-Ara*f*-(1→	5.09	4.06	3.81	4.15	3.57/3.69			
	110.61	83.04	77.61	80.41	62.32			
H → 3,5)-α-L-Ara*f*-(1→	5.01	3.99	3.89	4.17	3.66/3.75			
	108.53	82.41	85.28	83.47	67.59			
I → 5)-α-L-Ara*f*-(1→	4.96	3.99	3.88	4.17	3.66/3.75			
	108.68	82.37	77.77	83.47	67.59			

at δ_C 54.16 ppm represented the methyl carbon attached to the C-6 position in the methyl-esterified GalA residue (Petersen, et al., 2008). These characteristic signals indicated the presence of -COOMe in GalA residue, thus the sugar residue B has been recognized as → 4)-α-D-Gal*p*A-6-OMe-(1 →.

In the HMBC spectrum (Fig. 1F), a variety of residue connections can be inferred. The OMe/B C-6, A H-1/C/C^{-2}, C H-1/A/C^{-4}, A H-5/A/C^{-6}, G H-1/H C-3, H H-1/I C-5, I H-1/E C-3, E H-1/D C-6, F H-1/E C-3, and F H-1/H C-5 were recognized as the linkages of −6-OMe-(1 → 4)-α-D-Gal*p*A-6-OMe-(1→, →4)-α-Gal*p*A-(1 → 2,4)-α-L-Rha*p*-(1→ (A-C), →2,4)-α-L-Rha*p*-(1 → 4)-α-Gal*p*A-(1→ (C-A), →4)-α-Gal*p*A-(1 → 4)-α-Gal*p*A-(1→ (A-A), α-L-Ara*f*-(1 → 3,5)-α-L-Ara*f*-(1→ (G-H), →3,5)-α-L-Ara*f*-(1 → 5)-α-L-Ara*f*-(1→ (H-I), →5)-α-L-Ara*f*-(1 → 3,6)-β-D-Gal*p*-(1→ (I-E), →3,6)-β-D-Gal*p*-(1 → 6)-β-D-Gal*p*-(1→ (E-D), β-D-Gal*p*-(1 → 3,6)-β-D-Gal*p*-(1→ (F-E), β-D-Gal*p*-(1 → 3,5)-α-L-Ara*f*-(1→ (F-H), respectively. And in the NOESY spectrum (Fig. 1G), certain inter-residual cross-peaks were also identifed: the A H-1/A H-4, C H-1/A H-4, and D H-1/C H-4, suggesting that the linkages of → 4)-α-Gal*p*A-(1 → 4)-α-Gal*p*A-(1→ (A-A), →2,4)-α-L-Rha*p*-(1 → 4)-α-Gal*p*A-(1→ (C-A), →6)-β-D-Gal*p*-(1 → 2,4)-α-L-Rha*p*-(1→ (D-C) existed.

Consequently, the hypothetical structure of TFPS-1-3p was proposed as shown in Fig. 1H. TFPS-1-3p is a polysaccharide with the main linkage of [→4)-α-D-Gal*p*A(-6-OMe)-(1 → 4)-α-Gal*p*A-(1 →] and [→4)-α-D-Gal*p*A(-6-OMe)-(1 → 2,4)-α-L-Rha*p*-(1 →] and the branched chains including the linkage of → 6)-β-D-Gal*p*-(1 → and → 3,6)-β-D-Gal*p*-(1 → linkages) and (→5)-α-L-Ara*f*-(1 → and → 3,5)-α-L-Ara*f*-(1 →. There is a small amount of methyl esterification and *O*-2 or *O*-3 acetylated substitutions in the backbone of TFPS-1-3p. Similarly, given that most TFPS are mainly composed of Rha, Ara, GalA and Gal with small amounts of Glc, GalA, Xyl, depending on the extraction and separation method (Chen, Chen, Sun, Zeng, & Ye, 2020). The chemical structure of two purified TFPS fractions (namely TFPS-1 and TFPS-2) has been reported previously (Han, et al., 2011). Hereinto, TFPS-1 (167.5 kDa) contained α-L-Rha*p*, α-D-Gal*p*, α-D-Gal*p*A, α-D-Xyl*p*, α-D-Glc*p* and β-D-Glc*p* residues. TFPS-2 (10.1 kDa) was built from α-L-Rha*p*, α-L-Ara*p*, αD-Xyl*p*, α-D-Glc*p*, and α-D-Glc*p*A residues. It has been reported that structural characteristics could give rise to differences in the degradation process and bioactivity of polysaccharides. In particular, complex polysaccharides are theoretically difficult to be degraded thus could reach to the distal gut as a "prebiotic". Thus, the degradation properties and the effect of TFPS-1-3p on the gut microenvironment deserve to be addressed.

3.4. In vitro digestive properties of TFPS-1-3p

As shown in Table 3, there was no significant difference ($p > 0.05$) on the content of residual total carbohydrates and reducing sugars during the simulated saliva and gastrointestinal fluid digestion, indicating that TFPS-1-3p cannot be degraded by human saliva and gastrointestinal fluid. α-Amylase is the predominant active enzyme in saliva, capable of breaking the α-(1 → 4) linkages between glucose residues in starch and glycogen (Roberts & Whelan, 1960). Digestive enzymes in the human gastrointestinal digestive tract, including pepsin, lipase, and pancreatic enzymes, have a limited ability to degrade polysaccharides with complex linkage bonds (Brodkorb, et al., 2019). It was similar to the majority of plant-derived polysaccharides, such as from Fuzhuan brick tea (Chen, et al., 2017) and Chinese wolfberry (Zhou, et al., 2018), which structurally did not contain glycan α-(1 → 4) linkage and thus cannot be degraded by human saliva and gastrointestinal fluid. Subsequently, the TFPS-1-3p that has escaped depolymerization by enzymes of the upper human digestive system could safely reach the colon. The levels of residual total carbohydrates and reducing sugars were significantly lower during the fermentation phase ($p < 0.05$). These results suggested that TFPS-1-3p could be exploited by gut microbes. It has been widely recognized that gut microbes have the ability to encode a large number of CAZymes specifically designed to break down undigested polysaccharides as nutrients for their own growth has been widely recognized (Ndeh & Gilbert, 2018). A plausible hypothesis is that TFPS-1-3p was a dietary nutrient of the gut microbiota and was involved in regulating the gut microenvironment during the colonic fermentation.

Table 3
The content of residual total carbohydrate and reducing sugars during the *in vitro* gastrointestinal digestion and colonic fermentation process.

Process	Duration (h)	Total residual carbohydrate (%)	The residual reducing sugars (%)
Oral phase	0	100.00 ± 0.35a*	100.00 ± 3.01a
	0.5	100.37 ± 0.53a	98.74 ± 3.86a
	1	99.42 ± 0.46a	96.80 ± 3.98a
Gastric phase	0	100.00 ± 0.21a	100.00 ± 2.14a
	2	99.75 ± 0.03a	98.15 ± 6.12a
	6	99.87 ± 0.54a	98.60 ± 7.73a
Intestinal phase	0	100.00 ± 0.29a	100.00 ± 3.31a
	2	100.13 ± 0.32a	100.00 ± 4.73a
	6	99.92 ± 0.23a	99.89 ± 2.04a
Colonic phase	0	100.00 ± 0.39a	100.00 ± 1.70a
	6	85.43 ± 0.34b	86.76 ± 3.13b
	12	70.67 ± 0.26c	78.59 ± 3.40c
	24	42.44 ± 0.11d	52.35 ± 2.51d

*Different letters indicate significant differences between data within the same column ($p < 0.05$).

3.5. Effects of TFPS-1-3p on gut microenvironment

Emerging studies have found that the benefits of consuming a high-fiber diet are that gut microbes can metabolize indigestible polysaccharides to create SCFAs., thereby lowering the intracellular pH, and thus improving the gut microenvironment and body health (Lee, et al., 2022). SCFAs including lactate, acetate, propionate, *n*/*i*-butyrate and *n*/*i*-valerate, are the major metabolites of polysaccharides produced by gut microbiota. Currently, the levels of lactate, acetate, propionate, *n*/*i*-butyrate and *n*/*i*-valerate were measured during the colonic fermentation phase to evaluate the effects of TFPS-1-3p on the gut microenvironment and to provide further evidence for the degradation of TFPS-1-3p by gut microbiota. As the results were shown in Table 4, the levels of SCFAs enhanced with increasing fermentation time, among which acetate, propionate, and *n*-butyrate were the predominant metabolites. The concentrations of acetate and *n*-butyrate were significantly higher in the TFPS-1-3p group than in the BLK and FOS groups at different fermentation times ($p < 0.05$). Propionate and *n*-valerate appeared in all groups after 12 h of fermentation, and *i*-valerate and *i*-butyrate appeared after 24 h of fermentation, but propionate, *i*-butyrate, *i*-valerate and *n*-valerate were not detected in the Origin group and each treatment group after 6 h of fermentation. The content of total acids in the TFPS-1-3p group was higher than in the FOS and BLK groups at all stages of the fermentation process. In particular, after 24 h of fermentation, the total acids content of the TFPS-1-3p group (63.10 ± 0.46 mmol/L) was almost twice as high as that of the FOS group (33.30 ± 1.30 mmol/L) and three times as high as that of the BLK group (21.12 ± 0.83 mmol/L). SCFAs have been extensively implicated in the prevention of gut diseases and maintenance of gut health by modulating the immune system, lowering luminal pH to inhibit pathogenic intestinal bacteria, and boosting the mineral bioavailability (such as calcium and magnesium) (van der Hee & Wells, 2021). Additionally, Table 4 showed that the pH values of the FOS and BLK groups decreased significantly from 0 to 6 h, and then did not decrease further by increasing the fermentation time. Meanwhile, pH value gradually decreased within 24 h, which was in agreement with the downward trend of residual sugar content in the TFPS-1-3p group. Consequently, TFPS-1-3p can be released slowly to regulate the gut microenvironment without sudden changes in a short period of time.

The gut microbiota is a large colony of microorganisms' resident in the gut ecosystem, whose role in human health is to maintain a dynamic balance with the host and to play local and distant roles in key physiological processes. Polysaccharides are the most common nutritional

Table 4
The concentrations of SCFAs and the pH value during the colonic fermentation.

Duration (h)	Treatment	SCFAs (mmol/L)								pH value
		Lactate	Acetate	Propionate	*i*-Butyrate	*n*-Butyrate	*i*-Valerate	*n*-Valerate	Total acids	
0	Origin	1.00 ± 0.01f*	7.41 ± 0.02a	-#	–	1.77 ± 0.03a	–	–	10.18 ± 0.05a	7.00 ± 0.01f
6	FOS	2.53 ± 0.01i	11.82 ± 0.13e	–	–	2.29 ± 0.07b	–	–	16.65 ± 0.98 cd	4.62 ± 0.02a
	BLK	0.75 ± 0.06e	8.24 ± 0.36b	–	–	2.60 ± 0.07c	–	–	11.59 ± 0.85b	6.61 ± 0.02e
	TFPS-1-3p	0.82 ± 0.07e	13.60 ± 0.89f	–	–	4.85 ± 0.09e	–	–	19.26 ± 0.74de	6.04 ± 0.01d
12	FOS	1.99 ± 0.02 h	12.24 ± 0.82de	1.34 ± 0.03a	–	2.43 ± 0.10bc	–	1.27 ± 0.07b	18.28 ± 0.62d	4.65 ± 0.02a
	BLK	0.26 ± 0.02c	9.97 ± 0.29c	1.00 ± 0.08a	–	2.80 ± 0.11 cd	0.42 ± 0.02b	0.85 ± 0.02a	15.28 ± 0.93c	6.62 ± 0.02e
	TFPS-1-3p	0.33 ± 0.00d	20.50 ± 1.00 g	1.19 ± 0.12a	–	8.50 ± 0.11f	–	1.47 ± 0.09c	31.98 ± 0.92 g	5.60 ± 0.01c
24	FOS	1.81 ± 0.02 g	13.94 ± 0.69f	12.17 ± 0.57d	0.03 ± 0.00a	2.36 ± 0.19b	0.32 ± 0.01a	2.67 ± 0.04d	33.29 ± 1.30 g	4.68 ± 0.02a
	BLK	0.03 ± 0.00a	10.22 ± 0.94 cd	4.46 ± 0.31b	0.74 ± 0.04c	2.89 ± 0.09d	1.54 ± 0.04d	1.23 ± 0.00b	21.12 ± 0.83f	7.67 ± 0.08 g
	TFPS-1-3p	0.12 ± 0.02b	37.70 ± 0.28 h	6.69 ± 0.38c	0.54 ± 0.04b	14.21 ± 0.20 g	0.82 ± 0.01c	3.02 ± 0.04e	63.10 ± 0.46 h	5.40 ± 0.01b

#Not detected.
*Different letters indicate significant differences between data within the same column ($p < 0.05$).

components of the gut microbiome and are intimately involved in host wellness (Brodkorb, et al., 2019). During colonic fermentation, polysaccharides drive the growth of specified beneficial gut bacteria, modify the gut microbial profile, and alter local and remote host physiology to reduce disease incidence (Ho Do, Seo, & Park, 2021). In this paper, the effect of TFPS-1-3p on gut microbes was monitored by 16S rDNA high-throughput sequencing analysis. A totally 1,240,460 valid reads were acquired from 20 samples (62,023 ± 2,628 reads per sample). α-diversity refers to the average species diversity within a sample in the environment. The Sobs and Shannon indices are commonly used to reflect species α-diversity, and their values are proportional to community richness and diversity, respectively. As shown in Fig. 2A, the Sobs and Shannon indices of both the FOS and TFPS-1-3p groups were significantly lower than those of the BLK and Origin groups ($p < 0.05$), indicating that microbial fermentations of FOS and TFPS-1-3p were unable to increase community richness and diversity. This was in accordance with that described by (Zhou, et al., 2018), which was due to the selective induction of proliferation of specific microorganisms by FOS and TFPS-1-3p.

To obtain a clearer picture of the specific species variation, the LEfSe analysis, an indicator of β-diversity, was used to reveal taxonomic differences between treatments. As shown in Fig. 2B, the dominant taxa in the Origin group were Lentisphaerae and Candidatus_Saccharibacteria, Actinomycetaceae, Micrococcaceae, Bacillales_Incertae_Sedis_XI, Prevotellaceae, Enterococcaceae, Leuconostocaceae, Streptococcaceae, Clostridiaceae_1, Clostridiales_Incertae_Sedis_XI, Clostridiales_Incertae_Sedis_XIII, Eubacteriaceae, Peptostreptococcaceae, Ruminococcaceae, Victivallaceae, Methylobacteriaceae, Oxalobacteraceae, Pasteurellaceae and Moraxellaceae. The dominant species in the BLK group were Bacteroidetes, Proteobacteria, Fusobacteria, Synergistetes, Bacteroidaceae, Porphyromonadaceae, Acidaminococcaceae, Fusobacteriaceae, Desulfovibrionaceae, Succinivibrionaceae, Enterobacteriaceae and Synergistaceae. The dominant species in the FOS group were Bifidobacteriaceae, Rikenellaceae, Erysipelotrichaceae, Veillonellaceae and Sutterellaceae. While the dominant species in the TFPS-1-3p group were Coriobacteriaceae and Lachnospiraceae. Furthermore, the variation of microbes at the species level were shown in Fig. 2C. A total of 14 species of gut microorganisms differed significantly among the different groups. *Faecalibacterium prausnitzii* is one of the most predominant anaerobic strains in the human gut and has been shown to be a powerful probiotic for fight against inflammatory bacteria (Parsaei, Sarafraz, Moaddab, & Ebrahimzadeh Leylabadlo, 2021). A previous study revealed that *F. prausnitzii* could be enhanced by fermenting high-methoxyl pectins rather than low-methoxyl pectins (Larsen, et al., 2019). *F. prausnitzii* is capable of the acquisition and degradation of various β-mannooligosaccharides (Lindstad Lars, et al., 2021). However, *in vitro* culture and passage through the rough conditions of the gastrointestinal tract posed many difficulties due to its extremely sensitive characteristic (Phùng, et al., 2022). In this study, *F. prausnitzii* was significantly decreased ($p < 0.05$) after 24 h of *in vitro* fermentation in comparison to the Origin group. Additionally, TFPS-1-3p fermentation significantly reduced ($p < 0.05$) the relative abundance of *F. prausnitzii* when compared to the other groups. The limitation of *F. prausnitzii* after TFPS-1-3p fermentation might be associate with its structural characteristics, which is not abundant in β-mannooligosaccharides. Conversely, the relative abundance of *Fusobacterium mortiferum, Megasphaera elsdenii DSM 20460, Collinsella aerofaciens, Bacteroides thetaiotaomicron* and *Bacteroides plebeius* increased significantly ($p < 0.05$) after 24 h of TFPS-1-3p fermentation compared to the Origin and FOS groups, which may be related to the degradation of TFPS-1-3p. *Bacteroides* spp. is the mainstay in the human gut microbiota for metabolizing complex polysaccharides in the diet, dedicating up to 20 % of its genome to complex polysaccharide metabolism in the form of genes encoding primarily CAZymes such as polysaccharide lyases, glycoside hydrolases, polysaccharide transport and binding proteins, and carbohydrate sulfate lyases (Hindson, 2019). A versatile core genetic locus was found toorchestrate the metabolism of multiple glycans by *B. thetaiotaomicron* (Ndeh, et al., 2020). Similarly, *B. plebeius* have gained polysaccharide utilization loci enabling the hybrid galactan metabolism (Robb, et al., 2022). *F. mortiferum* has long been shown to encode 6-phospho-alpha-glucosidase (EC 3.2.1.122) that belongs to Family 4 of the glycosylhydrolase (Bouma, Reizer, Reizer, Robrish, & Thompson, 1997). Subsequently, the degradation products or fragments of TFPS-1-3p were converted into SCFAs. *M. elsdenii DSM 20460* can convert metabolites of other microorganisms (for example, *Trichoderma reesei* could secrete cellulase to degrade cellulose into soluble sugars) into various SCFAs (Shahab, et al., 2020). The fact that *C. aerofaciens* was one of the butyrate-producing bacteria was proved (Qin, et al., 2019). Therefore, *F. mortiferum, M. elsdenii DSM 20460, B. thetaiotaomicron, B. plebeius* and *C. aerofaciens* probably contributed to the degradation of the undigested heteropolysaccharide TFPS-1-3p and thus the gut microenvironment was modulated. However, the degradation pathways and polysaccharide

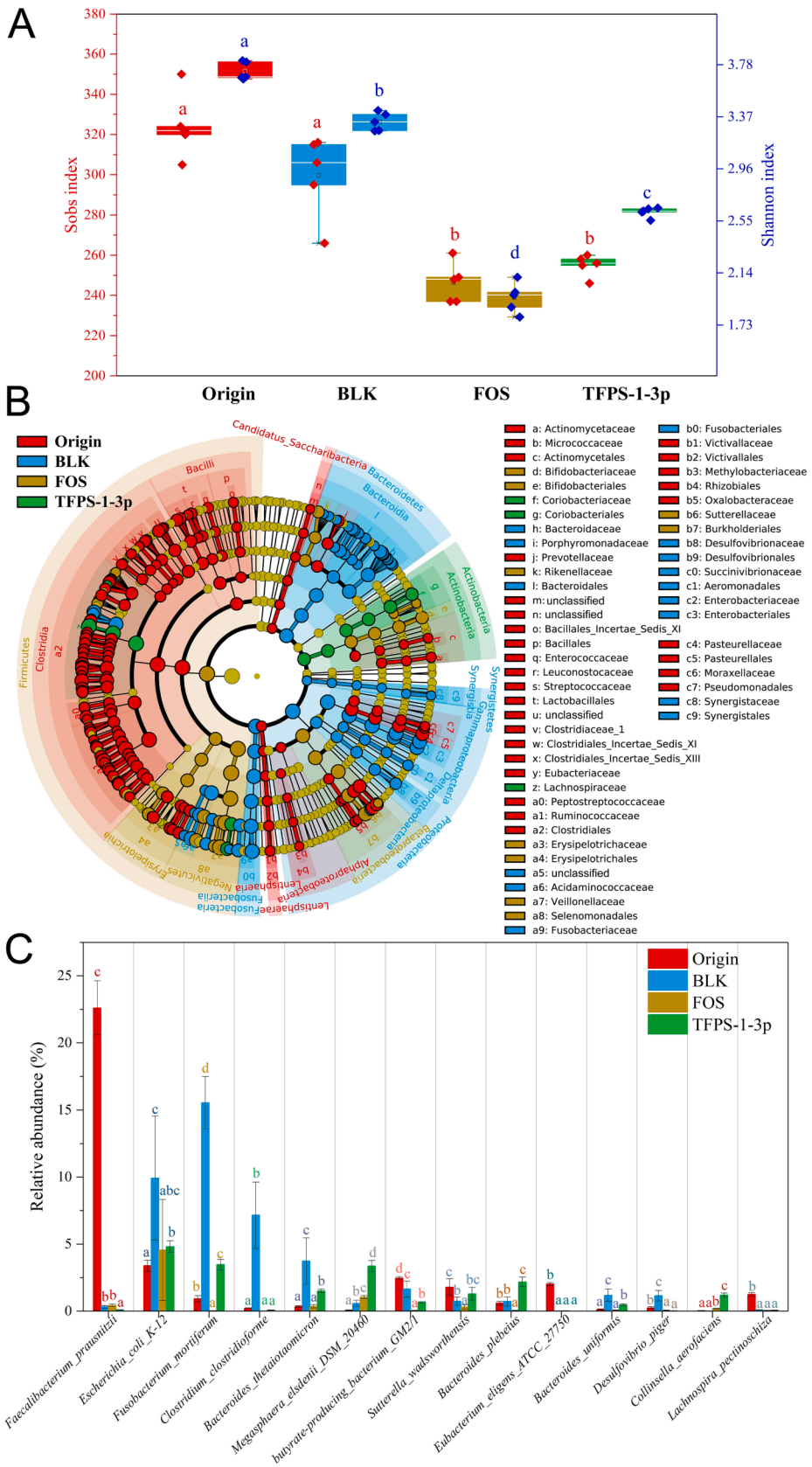

Fig. 2. The composition and diversity of gut microbiota. (A) α-diversity (Sobs and Shannon) indices, (B) LEfSe analysis, (C) Relative abundance of differentiated taxa at the species level. Different letters marked on the box (A) or column (C) within the same color indicate significant differences at $p < 0.05$ by Tukey test.

utilization loci of TFPS-1-3p need to be further explored.

4. Conclusion

TFPS-1-3p that was isolated from TFPS was a typical heteropolysaccharide with a molecular weight of 47.77 kDa. The linkages of TFPS-1-3p mainly contained → 4)-α-D-Gal*p*A(-6-OMe)-(1 → 4)-α-Gal*p*A-(1 → and → 4)-α-D-Gal*p*A(-6-OMe)-(1 → 2,4)-α-L-Rha*p*-(1 → with a little methyl esterification and (*O*-2 or *O*-3) acetylated substitutions. The branched chains consisted of linkages of → 6)-β-D-Gal*p*-(1 → and → 3,6)-β-D-Gal*p*-(1 → linkages) and (→5)-α-L-Ara*f*-(1 → and → 3,5)-α-L-Ara*f*-(1 →. TFPS-1-3p was resistant to degradation under simulated human gastrointestinal conditions but was degradable after *in vitro* colon fermentation. Thus, the gut microenvironment was changed with decreased pH and enhanced production of SCFAs, and the composition of the gut microbiota was altered. *F. mortiferum, M. elsdenii DSM 20460, B. thetaiotaomicron*, *B. plebeius* and *C. aerofaciens* potentially contributed to the degradation of TFPS-1-3p.

CRediT authorship contribution statement

Dan Chen: Project administration, Writing – original draft, Writing – review & editing, Funding acquisition. **Ao Wang:** Data curation, Investigation. **Jialiang Lv:** Validation, Visualization. **Chao Tang:** Supervision. **Chang-hai Jin:** Methodology. **Jun Liu:** Data curation. **Xiaoxiong Zeng:** Conceptualization, Resources. **Li Wang:** Funding acquisition.

Declaration of competing interest

The authors declare that they have no known competing financial interests or personal relationships that could have appeared to influence the work reported in this paper.

Data availability

Data will be made available on request.

Acknowledgments

This study was supported by the National Natural Science Youth Foundation of China (32102027), Anhui Natural Science Youth Foundation (2108085QC144), Natural Science Research Project of Colleges and Universities in Anhui Province (KJ2021A0143), Natural Science Youth Foundation of Anhui Agricultural University (2020zd17), Introduction and Stabilization Project of Talent Project of Anhui Agricultural University (rc352006), Shennong New Talent Project of Anhui Agricultural University (rc352102), and Scientific research start-up fee of Yangzhou University (137012022).

Appendix A. Supplementary data

Supplementary data to this article can be found online at https://doi.org/10.1016/j.fochx.2023.101058.

References

Bouma, C. L., Reizer, J., Reizer, A., Robrish, S. A., & Thompson, J. (1997). 6-phospho-alpha-D-glucosidase from Fusobacterium mortiferum: Cloning, expression, and assignment to family 4 of the glycosylhydrolases. *Journal of Bacteriology, 179*(13), 4129–4137.

Briggs, J. A., Grondin, J. M., & Brumer, H. (2021). Communal Living: Glycan Utilization by the Human Gut Microbiota. *Environmental Microbiology, 23*(1), 15–35.

Brodkorb, A., Egger, L., Alminger, M., Alvito, P., Assunção, R., Ballance, S., … Recio, I. (2019). INFOGEST static *in vitro* simulation of gastrointestinal food digestion. *Nature Protocols, 14*(4), 991–1014.

Chen, D., Chen, G. J., Sun, Y., Zeng, X. X., & Ye, H. (2020). Physiological genetics, chemical composition, health benefits and toxicology of tea (Camellia sinensis L.) flower: A review. *Food Research International, 137*, Article 109584.

Chen, D., Chen, G. J., Ding, Y., Wan, P., Peng, Y. J., Chen, C. X., … Ran, L. W. (2019). Polysaccharides from the flowers of tea (Camellia sinensis L.) modulate gut health and ameliorate cyclophosphamide-induced immunosuppression. *Journal of Functional Foods, 61*, Article 103470.

Chen, G. J., Bai, Y. X., Zeng, Z. Q., Peng, Y. J., Zhou, W. T., Shen, W. B., … Liu, Z. H. (2021). Structural Characterization and Immunostimulatory Activity of Heteropolysaccharides from Fuzhuan Brick Tea. *Journal of Agricultural and Food Chemistry, 69*(4), 1368–1378.

Chen, G. J., Xie, M. H., Wan, P., Chen, D., Ye, H., Chen, L. G., … Liu, Z. H. (2017). Digestion under saliva, simulated gastric and small intestinal conditions and fermentation *in vitro* by human intestinal microbiota of polysaccharides from Fuzhuan brick tea. *Food Chemistry, 244*, 331–339.

Chen, R. X., Xu, J. X., Wu, W. H., Wen, Y. X., Lu, S. Y., El-Seedi, H. R., & Zhao, C. (2022). Structure-immunomodulatory activity relationships of dietary polysaccharides. *Current Research in Food Science, 5*, 1330–1341.

de Vos, W. M., Tilg, H., Van Hul, M., & Cani, P. D. (2022). Gut microbiome and health: Mechanistic insights. *Gut, 71*(5), 1020–1032.

Dubois, M., Gilles, K. A., Hamilton, J. K., Rebers, P. A., & Smith, F. (1956). Colorimetric method for determination of sugars and related substances. *Analytical Chemistry, 28*(3), 350–356.

Fan, Y., & Pedersen, O. (2021). Gut microbiota in human metabolic health and disease. *Nature Reviews Microbiology, 19*(1), 55–71.

Frampton, J., Murphy, K. G., Frost, G., & Chambers, E. S. (2020). Short-chain fatty acids as potential regulators of skeletal muscle metabolism and function. *Nature Metabolism, 2*(9), 840–848.

Han, Q., Yu, Q. Y., Shi, J., Xiong, C. Y., Ling, Z. J., & He, P. M. (2011). Structural Characterization and Antioxidant Activities of 2 Water-Soluble Polysaccharide Fractions Purified from Tea (Camellia sinensis) Flower. *Journal of Food Science, 76*(3), C462–C471. https://doi.org/10.1111/j.1750-3841.2011.02063.x

Hasain, Z., Mokhtar, N. M., Kamaruddin, N. A., Mohamed Ismail, N. A., Razalli, N. H., Gnanou, J. V., & Raja Ali, R. A. (2020). Gut microbiota and gestational diabetes mellitus: A review of host-gut microbiota interactions and their therapeutic potential. *Frontiers in Cellular and Infection Microbiology, 10*, 188.

Hindson, J. (2019). *Bacteroides* compete for fibre-derived glycans. *Nature Reviews Gastroenterology & Hepatology, 16*(12), 706–707.

Ho Do, M., Seo, Y. S., & Park, H.-Y. (2021). Polysaccharides: Bowel health and gut microbiota. *Critical Reviews in Food Science and Nutrition, 61*(7), 1212–1224. https://doi.org/10.3389/fmicb.2019.00223

Langille, M. G. I., Zaneveld, J., Caporaso, J. G., McDonald, D., Knights, D., Reyes, J. A., … Huttenhower, C. (2013). Predictive functional profiling of microbial communities using 16S rRNA marker gene sequences. *Nature Biotechnology, 31*, 814–823.

Larsen, N., Bussolo de Souza, C., Krych, L., Barbosa Cahú, T., Wiese, M., Kot, W., … Jespersen, L. (2019). Potential of Pectins to Beneficially Modulate the Gut Microbiota Depends on Their Structural Properties. *Frontiers in Microbiology, 10*. https://doi.org/10.3389/fmicb.2019.00223

Lee, H.-B., Kim, Y.-S., & Park, H.-Y. (2022). Pectic polysaccharides: Targeting gut microbiota in obesity and intestinal health. *Carbohydrate Polymers, 287*, Article 119363.

Lindstad Lars, J., Lo, G., Leivers, S., Lu, Z., Michalak, L., Pereira Gabriel, V., … La Rosa Sabina, L. (2021). Human gut *Faecalibacterium prausnitzii* deploys a highly efficient conserved system to cross-feed on β-Mannan-derived oligosaccharides. *MBio, 12*(3), e03620–e3628.

Miller, G. L. (1959). Use of dinitrosalicylic acid reagent for determination of reducing sugar. *Analytical Chemistry, 31*(3), 426–428.

Ndeh, D., Basle, A., Strahl, H., Yates, E. A., McClurgg, U. L., Henrissat, B., … Cartmell, A. (2020). Metabolism of multiple glycosaminoglycans by *Bacteroides thetaiotaomicron* is orchestrated by a versatile core genetic locus. *Nature Communications, 11*(1), 646.

Ndeh, D., & Gilbert, H. J. (2018). Biochemistry of complex glycan depolymerisation by the human gut microbiota. *Fems Microbiology Reviews, 42*(2), 146–164.

Parsaei, M., Sarafraz, N., Moaddab, S. Y., & Ebrahimzadeh Leylabadlo, H. (2021). The importance of *Faecalibacterium prausnitzii* in human health and diseases. *New Microbes and New Infections, 43*, Article 100928.

Patova, O. A., Smirnov, V. V., Golovchenko, V. V., Vityazev, F. V., Shashkov, A. S., & Popov, S. V. (2019). Structural, rheological and antioxidant properties of pectins from *Equisetum arvense* L. and *Equisetum sylvaticum* L. *Carbohydrate Polymers, 209*, 239–249.

Petersen, B. O., Meier, S., Duus, J.Ø., & Clausen, M. H. (2008). Structural characterization of homogalacturonan by NMR spectroscopy-assignment of reference compounds. *Carbohydrate Research, 343*(16), 2830–2833.

Phùng, T.-T.-T., Geremetta, M., Chanut, J., Raise, A., Ureña, M., Dupont, S., … Karbowiak, T. (2022). Comprehensive approach to the protection and controlled release of extremely oxygen sensitive probiotics using edible polysaccharide-based coatings. *International Journal of Biological Macromolecules, 218*, 706–719.

Qin, P. P., Zou, Y. Q., Dai, Y., Luo, G. W., Zhang, X. W., & Xiao, L. (2019). Characterization a Novel Butyric Acid-Producing Bacterium *Collinsella aerofaciens* Subsp. *Shenzhenensis Subsp. Nov. Microorganisms, 7*(3), 78.

Robb, C. S., Hobbs, J. K., Pluvinage, B., Reintjes, G., Klassen, L., Monteith, S., Giljan, G., Amundsen, C., Vickers, C., Hettle, A. G., Hills, R., Nitin, Xing, X., Montina, T., Zandberg, W. F., Abbott, D. W., & Boraston, A. B. (2022). Metabolism of a hybrid algal galactan by members of the human gut microbiome. *Nature Chemical Biology, 18*(5), 501-510.

Roberts, P. J. P., & Whelan, W. J. (1960). The mechanism of carbohydrase action. 5. Action of human salivary α-amylase on amylopectin and glycogen. *Biochemical Journal, 76*(2), 246–253.

Shahab, R. L., Brethauer, S., Davey, M. P., Smith, A. G., Vignolini, S., Luterbacher, J. S., & Studer, M. H. (2020). A heterogeneous microbial consortium producing short-chain fatty acids from lignocellulose. *Science, 369*(6507), eabb1214.

Sims, I. M., Carnachan, S. M., Bell, T. J., & Hinkley, S. F. R. (2018). Methylation analysis of polysaccharides: Technical advice. *Carbohydrate Polymers, 188*, 1–7.

Tang, C., Ding, R., Sun, J., Liu, J., Kan, J., & Jin, C. (2019). The impacts of natural polysaccharides on intestinal microbiota and immune responses-a review. *Food & Function, 10*(5), 2290–2312.

Tian, L., Bruggeman, G., Van, d. B. M., Borewicz, K., Scheurink, A. J., Bruininx, E., De, V. P., Smidt, H., Schols, H. A., & Gruppen, H. (2016). Effects of pectin on fermentation characteristics, carbohydrate utilization and microbial community composition in the gastrointestinal tract of weaning pigs. *Molecular Nutrition & Food Research*. https://doi.org/10.1002/mnfr.201600186.

van der Hee, B., & Wells, J. M. (2021). Microbial regulation of host physiology by short-chain fatty acids. *Trends in Microbiology, 29*(8), 700–712.

Yao, H. Y. Y., Wang, J. Q., Yin, J. Y., Nie, S. P., & Xie, M. Y. (2021). A review of NMR analysis in polysaccharide structure and conformation: Progress, challenge and perspective. *Food Research International, 143*, Article 110290.

Yuan, Q. X., Zhang, J., Xiao, C. L., Harqin, C. L. G., Ma, M. Y., Long, T., … Zhao, L. Y. (2020). Structural characterization of a low-molecular-weight polysaccharide from *Angelica pubescens* Maxim. f. *biserrata* Shan et Yuan root and evaluation of its antioxidant activity. *Carbohydrate Polymers, 236*, Article 116047.

Yuan, Q. X., Zhao, L. Y., Cha, Q. Q., Sun, Y., Ye, H., & Zeng, X. X. (2015). Structural characterization and immunostimulatory activity of a homogeneous polysaccharide from *sinonovacula constricta*. *Journal of Agricultural and Food Chemistry, 63*(36), 7986–7994.

Zhou, W. T., Yan, Y. M., Mi, J., Zhang, H. C., Lu, L., Luo, Q., … Cao, Y. L. (2018). Simulated digestion and fermentation *in vitro* by human gut microbiota of polysaccharides from bee collected pollen of chinese wolfberry. *Journal of Agricultural and Food Chemistry, 66*(4), 898–907.